Journal Name

ARTICLE

A multifunctional magnetic material under pressure

Cite this: DOI: 10.1039/x0xx00000x

J. A. Rodríguez-Velamazán,[a,b,*] O. Fabelo,[a,b] C. M. Beavers,[c] E. Natividad,[a] M. Evangelisti,[a] O. Roubeau[a,*]

Received 00th January 2012,
Accepted 00th January 2012

DOI: 10.1039/x0xx00000x

$[Fe^{II}(Metz)_6](Fe^{III}Br_4)_2$ (Metz = 1-methyltetrazole) is one of the rare systems combining spin-crossover and long-range magnetic ordering. The spin-crossover phenomenon of the cationic sub-lattice $[Fe^{II}(Metz)_6]^{2+}$ coexists in this multifunctional material with an antiferromagnetic order of the anionic sub-lattice $(Fe^{III}Br_4)^-$. A combined study involving neutron and X-ray diffraction and bulk and single-crystal magnetometry allows determining the collinear antiferromagnetic structure of this system, and shows that the magnetic ordering is favoured by the application of pressure, with an increase of the Néel temperature from 2.4 K at ambient pressure, to 3.9 K at 0.95 GPa. Applied pressure also enables a full high-spin to low-spin switch at ambient temperature.

Introduction

The molecular approach for the design of multifunctional materials makes use of the flexibility offered by molecular systems for combining different functional properties in the same compound. Several recent examples illustrate the success of this approach, featuring e.g., magnetic and optical properties,[1] porosity and magnetism,[2] conductivity and magnetism,[3] superconductivity and magnetism,[4] or even a multiferroic character.[5] The spin crossover (SCO) phenomenon[6] is in itself a source of multifunctionality,[7] with drastic variations in magnetic, optical, dielectric and structural properties potentially taking place concomitantly with the change of spin state between high-spin (HS) and low-spin (LS) electronic configurations.[8] Conveniently, this molecular bistability can be addressed by an external perturbation[9] like temperature,[10] magnetic field,[11] light irradiation,[12] chemical stimuli[13] or pressure.[14] Very recent reports have in addition shown that the light-induced HS form of an Fe(II) SCO material can behave as a Single-Molecule Magnet (SMM) and that photomagnetic chains can be designed by linking SCO and SMM building blocks.[15] On the other hand, although magnetic ordering is one of the most pursued functional properties due to its potential use in a variety of applications,[16] the molecular-based systems combining it with SCO are still scarce. This combination has been achieved in hybrid crystalline solids that integrate Fe^{III} SCO centres together with Mn^{II}-Cr^{III}-oxalate-based magnetic networks.[17] In Fe^{II} SCO systems, which are particularly interesting since the involved LS state is diamagnetic, the combination of SCO and long range magnetic ordering remains more elusive. An exception is a recent Fe–Nb metal–organic framework featuring a light-induced magnetic ordering.[18]

$[Fe^{II}(Metz)_6](Fe^{III}Br_4)_2$ (Metz = 1-methyltetrazole)[19] (**1**) is in this respect an exciting new example combining SCO and magnetic order. The trigonal structure of **1** has one $[Fe(Metz)_6]^{2+}$ cation and two $FeBr_4^-$ anions in the unit cell, building hexagonal layers extended in the *ab* plane (Figure 1). These layers are pillared along the *c* axis, in a perfectly eclipsed conformation. According to magnetic and calorimetric measurements, $[Fe(Metz)_6]^{2+}$ cations present a gradual complete thermal SCO centred at 165 K, coexisting with a long range antiferromagnetic order below T_N = 2.4 K of the $FeBr_4^-$.[19] We report here the magnetic structure of this original material and present a detailed study of how applied pressure affects both the SCO and the magnetic order.

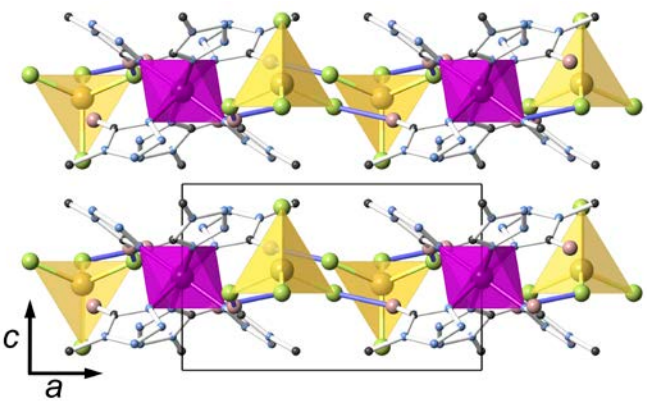

Figure 1. View along the *b* axis of the structure of **1** at 10 K – $[Fe(N)_6]$ polyhedra in purple, $FeBr_4^-$ anions in yellow, H···Br short contacts as blue sticks.

Results and discussion

The compound $[Fe^{II}(Metz)_6](Fe^{III}Br_4)_2$ was readily prepared as shiny red polycrystalline material, as previously reported.[19] Slower evaporation of the ethanolic solution containing the mixture of $FeBr_2$, $FeBr_3$ and Metz allows the formation of larger hexagonal rod-shape single crystals, suitable for single-crystal magnetic measurements (ESI). Bulk calorimetric and magnetic data clearly indicate the presence of an antiferromagnetic order of the $FeBr_4^-$ anionic sublattice in **1** below 2.4 K, in addition to the SCO of the $[Fe(Metz)_6]^{2+}$ cation observed at higher temperatures.[19] We have now used powder neutron diffraction (PND) and single-crystal magnetometry for determining the magnetic structure of **1**. A first high-resolution PND data collection aimed at refining the nuclear structure at low temperature has been performed at 10 K – with the cationic sublattice in the LS diamagnetic state and the anionic one in a paramagnetic state – using a wavelength of 1.59 Å (see ESI for full experimental and crystallographic details). The diffraction pattern essentially matches the reported structure determined by X-ray at 104 K,[19] although the better sensitivity of neutrons to hydrogen compared with X-rays reveals a rotation of the methyl groups of Metz that slightly changes the described hydrogen-bonding network, with shortened H···Br distances that create double-layered planes parallel to *ab* (Figure 1, Tables 1 and S2). The Rietveld refinement (Figure S1, Tables 1 and S1) shows also a small decrease of volume of ca. 2%, which can be assigned to thermal compression of the cell parameters.

Table 1. Cell parameters and relevant bond distances (Å) and angles (º) as well as short contacts (Å) in the structure of **1** at 10 K / ambient pressure and 298 K / 2.3 GPa. See Figure 5 for labelling. Data from the structures at ambient pressure and 298 K and 104 K are recalled for comparison.[19]

T, K	10(2)	298(2)	296(2)	104(2)
p, GPa	amb.	2.3	amb.	amb.
radiation	neutrons	X-rays	X-rays	X-rays
λ, Å	1.59	0.72930	0.71073	0.71073
crystal system		trigonal		
space group		*P*–3		
a, *b* Å	12.5957(1)	12.2039(14)	12.9487(1)	12.683(2)
c, Å	6.7659(1)	6.4241(7)	6.9577(1)	6.7890(14)
V, Å^3	929.61(2)	828.6(2)	1010.30(2)	947.0(3)
Fe1–N1	1.984(7)	1.952(3)	2.187(2)	2.003(2)
Fe2···Fe2#1	7.290(1)	7.0718(6)	7.489(1)	7.337(1)
Fe2···Fe2#2	6.7659(1)	6.4241(7)	6.9577(1)	6.7980(14)
Br2···H1A	2.65(3)	2.683(1)	2.911 (1)	2.807(1)

Symmetry operations: #1:1–x, 1–y, 1–z; #2: x, y, 1+z

Figure 2 shows the PND patterns collected at 1.5 and 4.5 K in the high-flux diffractometer D1B using a wavelength of 2.52 Å. At the lowest temperature, an increase of intensity in some nuclear Bragg reflections – (100), (101) / (011) – is noticed, indicating the appearance of long-range magnetic order. The observed magnetic contribution can be indexed with a magnetic propagation vector **k** = (0,0,0), that is, the magnetic unit cell coincides with the nuclear one.

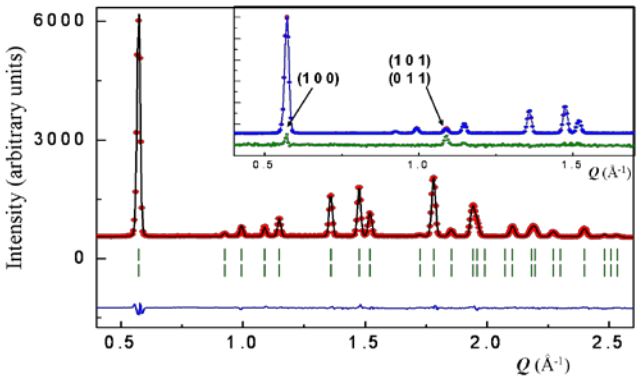

Figure 2. Powder neutron diffraction pattern of $[Fe(Metz)_6](FeBr_4)_2$ at ambient pressure collected at 1.5 K (red symbols) and Rietveld refinement (black line) with Bragg peak positions (green lines). Inset: Experimental patterns collected at ambient pressure at 1.5 K (red) and 4.5 K (blue). The difference diffraction pattern (green), which has been rescaled for clarity, stands for the contribution of the magnetic phase, with some characteristic reflections indicated.

The representational analysis technique described by Bertaut[20] has been used to determine the possible magnetic structures compatible with the *P*–3 space group of **1.** This gives four possible magnetic configurations considering the two magnetic Fe^{III} ions in the unit cell, namely (i) ferromagnetic with moments along *c*, (ii) antiferromagnetic with moments along *c*, (iii) ferromagnetic with moments in the *ab* plane, and (iv) antiferromagnetic with moments in the *ab* plane (it should be noted that PND is not sensitive, in the present symmetry, to the absolute orientation angle of the magnetic moments contained in the *ab* plane). In order to determine the magnetic configuration, we consider as a first approximation a fixed magnetic moment of 3.5 μ_B in each Fe^{III} site, in agreement with the expected value at 1.5 K for a Heisenberg 3D ordering of S = 5/2 spins and T_N = 2.4 K (see below) and we calculate the four possible magnetic structures to be compared against the experimental data. This comparison immediately reveals (see Figure S3) that the only configuration compatible with the data is antiferromagnetic with moments in the *ab* plane (configuration iv, Figure 3). In order to verify this result overcoming the symmetry restrictions, a simulated annealing method was applied,[21] using a spherical coordinate system to describe the orientation of the moment. With the magnetic moment of the Fe^{III} ions constrained, as previously, to a fixed value of 3.5 μ_B, but the spherical angles left free, the procedure always converges to a magnetic structure corresponding to moments almost exactly antiparallel and lying in the *ab* plane (Figure 3), thus confirming the previous result. Using this model, the Rietveld refinement with unconstrained magnetic moment (Figure 2) gives a value of 3.44 ± 0.25 μ_B (R_{mag}= 12.30 %). Single-crystal magnetic measurements (Figures S4-S6) fully agree with the *c* axis being a hard axis of magnetization and the *ab* plane an easy plane, as evidenced by *M* vs. *H* (Figure S5) and χ vs. *T* data (Figures 4 and S6). The latter also confirms the value of T_N = 2.4 K obtained on the bulk.[19]

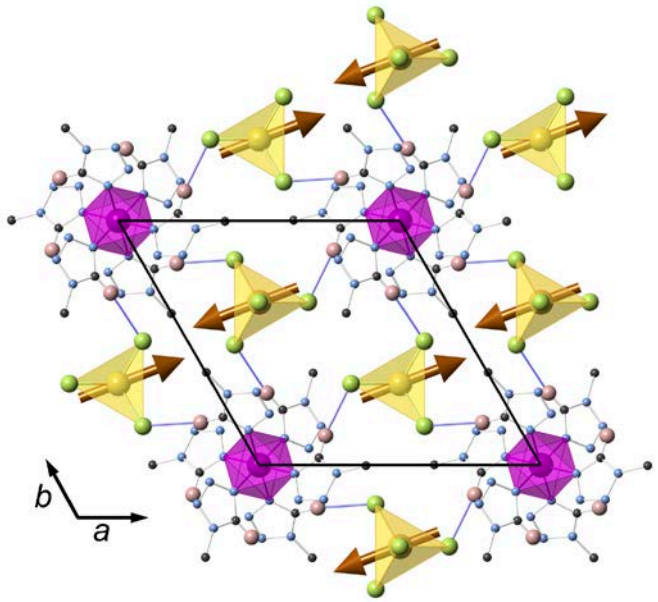

Figure 3. View of the magnetic structure of $[Fe(Metz)_6](FeBr_4)_2$. Same colour code as in Fig. 1. The moments' orientation in the *ab* plane is arbitrary (see text).

The neutron data are also in good agreement with this value of T_N since the intensity of the magnetic reflections decreases with temperature, vanishing between 2.3 and 2.45 K. The refined value of the magnetic moment correspondingly decreases (Figure 4), showing a temperature dependence that approximately follows a power-law Ct^{β} corresponding to a Heisenberg 3D ordering of S = 5/2 spins (with C = 5, $t = |T - T_N|$, T_N = 2.4 K, and β = 0.364),[22] as is expected for Fe^{III} ions. A 3D antiferromagnetic order in the same temperature range has indeed recently been reported in the plastic crystal choline$[FeCl_4]$,[23] although the absence of structural data impedes magneto-structural correlation in this case. The magnetic order in **1** finds its origin in two types of interactions among these Fe(III) spins. First, the 1D symmetric stacks of $FeBr_4^-$ anions gives rise to a direct *d-d* ferromagnetic exchange interaction[24] that we previously evaluated on basis of the Fe···Fe distance along the stacks at 104 K.[19,24] The shorter distance observed here in the 10 K structure provides a more accurate larger value of J/k_B = 0.32 K,[24] which is in excellent agreement with that derived from a Curie-Weiss fit (Figure S7).[25] The value of the critical temperature, T_N = 2.4 K, is a measure of the energy per spin involved in the ordering mechanism. Therefore, neglecting crystal-field interactions, since the intrachain energy is $|E_J| = JS^2$ = 2.0 K, there is a remaining 0.4 K that we associate to the inter-stack coupling, i.e. J'/k_B of the order of –0.09 K.[26] This weak though noticeable interaction could arise from exchange coupling through direct Br···Br contacts of the $FeBr_4^-$ ions within the *ab* plane (Table S2, Figure S8), but the fact that the magnetic moments are oriented perpendicular to the ferromagnetic chains would also be consistent with a magnetostatic (dipolar) origin for the antiferromagnetic order.[27] The estimation of the dipolar ground state yields $|E_{dip}|$ = 0.5 K,[28] thus making the latter hypothesis more plausible.

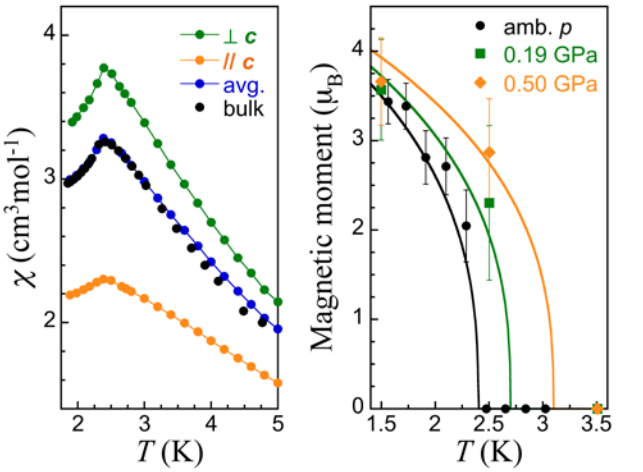

Figure 4. Left: Single-crystal molar magnetic susceptibility (χ) vs. T with 0.1 T dc field perpendicular (green) and parallel (orange) to the crystallographic *c* axis. The average χ (blue) compares well with bulk data (black). Right: temperature dependence of the magnetic moment obtained from PND at the indicated pressures. Solid lines are the power-law $C|T - T_N|^{\beta}$ with C = 5, β = 0.364, and T_N = 2.4 K (black), 2.7 K (green) and 3.1 K (orange).

As mentioned before, pressure is one of the external stimuli used for switching the spin state in SCO based multifunctional materials.[9] In the present case, besides the well-established stabilization of the LS state,[6] pressure would likely affect the low temperature magnetic properties as well, and could be a suitable external parameter for addressing the magnetic ordering of the complex. The crystal structure of **1** was thus determined at RT at a pressure of 2.3 GPa, using a Diamond Anvil Cell and synchrotron radiation (see ESI for details). An ellipsoid representation of the structure is provided in Figure 5, showing the $[Fe(Metz)_6]^{2+}$ cation and one $FeBr_4^-$ anion. Significant compression of the cell is observed (Tables 1 and S1), by ca. 18.6% in volume, and both *a* and *c* axis partake in the compression, being reduced by respectively 6.0 and 7.9 % at 12.2039(14) and 6.4241(7) Å. This results in a reduction of the $Fe^{III}\cdots Fe^{III}$ inter-layer separation within the $FeBr_4^-$ stacks, coinciding with the *c* parameter, as well as of the inner-layer distance, now at 7.072 Å (Table 1). The main structural change in the SCO cation regards the Fe–N bond length, reduced from 2.187(2) at ambient pressure to 1.952(3) Å, distance even shorter than for the LS state at 104 K, i.e. 2.003(2) Å (Table 1). This clearly indicates a full pressure-induced SCO, as confirmed by strong darkening of the crystal. Importantly the structure is similar in most aspects to that derived at 10 K from PND (Tables 1 and S2), including a similar orientation of the tetrazole ring resulting in shorter H···Br contacts, at 2.683(1) Å. This is particularly relevant as the average rotation of the tetrazole rings has been proposed to explain the site-specific stabilization of HS or LS states in a related compound with a partial SCO, i.e. $[Fe(Metz)_6](BF_4)_2$.[29]

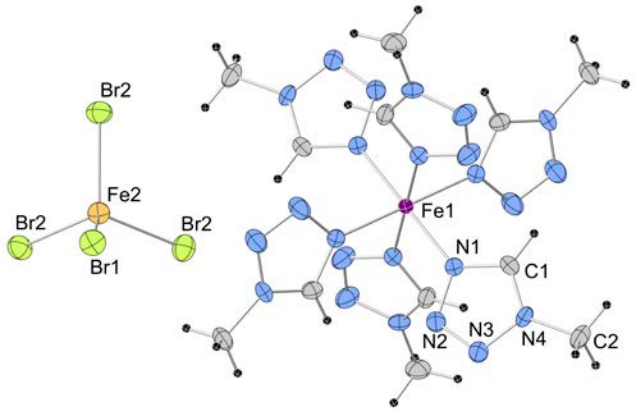

Figure 5. Structure of **1** at 2.3 GPa and 298 K, ellipsoids at 50 % probability. Colour code: Fe(II) purple, Fe(III) orange, Br light green, N blue, C, grey, H black.

Magnetic susceptibility (χ) measurements under pressure (Figure 6, ESI for details) confirm the structural observations, the SCO centred at 165 K at ambient pressure being shifted to 325 K at 0.8 GPa. This indicates that the spin-state of the Fe^{II} ion in **1** is in fact switched to LS at room temperature by only applying ca. 1 GPa. Moreover, as can be seen in Figure 6, the application of such pressures also affects the long-range magnetic ordering of **1**. The low temperature data at various applied pressures indeed evidence a shift towards higher temperatures and broadening of the maxima corresponding to the antiferromagnetic ordering of the $FeBr_4^-$ ions. The maxima in the curves mark the ordering temperature, T_N, that increases with pressure following a linear dependence (Figure 6). PND under applied pressure confirms the enhancement of the magnetic interaction revealed by this T_N increase. PND patterns collected at different temperatures between 1.5 and 10 K, and at applied pressures of 0.19 and 0.50 GPa are compatible with the same magnetic structure model described previously for ambient pressure (Figure S9). The increase of T_N is deduced from the fact that a significant magnetic moment can still be refined at 2.5 K, with values of 2.32 ± 0.86 μ_B (R_{mag}= 16.80 %) and 2.88 ± 0.60 μ_B (R_{mag}= 14.23 %) for 0.19 and 0.50 GPa respectively. As shown in Figure 4, these values are in agreement with the same power-law dependence proposed for ambient pressure, Ct^{β}, (C = 5, β = 0.364) just scaling to the appropriate T_N given by the susceptibility measurements (2.7 and 3.1 K for 0.19 and 0.50 GPa respectively). The increase of T_N with applied pressure is likely a joint effect of the structural modifications of the $FeBr_4^-$ ions packing. Indeed, both the ferromagnetic exchange interaction within the $FeBr_4^-$ ions along c and the antiferromagnetic dipolar interaction between these stacks in the ab plane are expected to increase with reduced $Fe^{III}\cdots Fe^{III}$ distances.[21,23] The effect of the former should however be dominant since the corresponding $Fe^{III}\cdots Fe^{III}$ distances along the c axis suffer a stronger reduction under pressure than those distances contained in the ab plane (–7.7% vs. –5.6%, Tables 1 and S2), and the exchange interaction is much more sensitive to distance variations (~ r^{-10}) than the dipolar interaction (~ r^{-3}).[30]

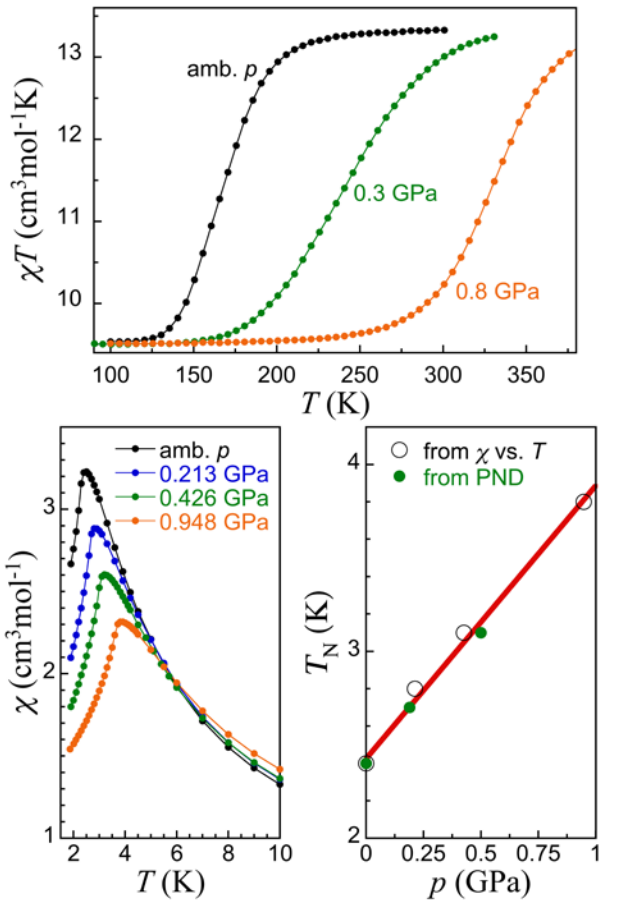

Figure 6. Top: Temperature dependence of the χT product (χ is the molar magnetic susceptibility) for **1** at the indicated pressures. Bottom left: Molar magnetic susceptibility of **1** as a function of temperature at the indicated pressures. Bottom right: pressure dependence of T_N. The red line is a linear fit of data derived from both magnetic susceptibility and PND.

Conclusions

In this work, we have successfully applied neutron diffraction and single-crystal magnetic measurements to determine the magnetic structure of $[Fe^{II}(Metz)_6](Fe^{III}Br_4)_2$, a unique multifunctional material presenting a magnetically-ordered phase at low temperatures as well as the spin-crossover phenomenon. The effect of applied pressure on the magnetic order has been determined and correlated with aspects of the X-ray structure determined at higher pressures. The latter also demonstrated the efficient spin-crossover induced by pressure at ambient temperature, which was corroborated by magnetic measurements. Altogether our results highlight the great potential of simple two-network hybrid spin crossover systems to provide original multifunctional materials

Acknowledgements

This work was supported by the Spanish MINECO and FEDER, projects MAT2011-24284 and MAT2011-27233-C02-02 and MAT2012-38318-C03-01. We are grateful to the Spanish CRG D1B and Institut Laue-Langevin for neutron

beam time allocation. The Advanced Light Source is supported by the Director, Office of Science, Office of Basic Energy Sciences of the U. S. Department of Energy under contract no. DE-AC02- 05CH11231. High pressure facilities at the Advanced Light Source are partially supported by COMPRES, the Consortium for Materials Properties Research in Earth Sciences, under NSF Cooperative Agreement EAR 11-57758.

Notes and references

[a] Instituto de Ciencia de Materiales de Aragón (ICMA), CSIC – Universidad de Zaragoza, 50009 Zaragoza, Spain.

[b] Institut Laue-Langevin, 38042 Grenoble Cedex 9, France.

[c] Advanced Light Source, Berkeley Laboratory, 1 Cyclotron Road, Berkeley 94720, USA.

† Electronic Supplementary Information (ESI) available: Experimental details, neutron and X-ray crystallographic data, additional magnetic susceptibility and magnetization measurements, high-resolution neutron powder diffraction pattern at 10 K and Rietveld refinement, and calculated diffraction patterns for the different magnetic models compared with the data. CCDC 983920 (**1**, 10 K, ambient pressure) and 983921 (**1**, 298 K, 2.3 GPa). See DOI: 10.1039/b000000x/

1 (a) O. Sato, *Acc. Chem. Res.*, 2003, **36**, 692; (b) Y. Sunatsuki, Y. Ikuta, N. Matsumoto, H. Ohta, M. Kojima, S. Iijima, S. Hayami, Y. Maeda, S. Kaizaki, F. Dahan and J. P. Tuchagues, *Angew. Chem. Int. Ed.*, 2003, **42**, 1614.

2 (a) D. Maspoch, D. Ruiz-Molina, K. Wurst, N. Domingo, M. Cavallini, F. Biscarini, J. Tejada, C. Rovira and J. Veciana, *Nat. Mater.*, 2003, **2**, 190; (b) D. Maspoch, D. Ruiz-Molina and J. Veciana, in Magnetism: Molecules to Materials V, Eds. J. S. Miller and M. Drillon, Wiley-VCH 2006, pp 261-282 and references therein; (c) M. Kurmoo, H. Kumagai, K. W. Chapman and C. J. Kepert, *Chem. Commun.*, 2005, 3012; (d) G. J. Halder, C. J. Kepert, B. Moubaraki, K. S. Murray and J. D. Cashion, *Science*, 2002, **298**, 1762.

3 (a) E. Coronado, J. R. Galan-Máscarós, C. J. Gómez-García and V. Laukhin, *Nature* 2000, **408**, 447; (b) E. Coronado, P. Day, *Chem. Rev.*, 2004, **104**, 5419. (c) H. Kobayashi, H-B. Cui and A. Kobayashi, *Chem. Rev.*, 2004, **104**, 5265.

4 E. Coronado, C. Martí-Gastaldo, E. Navarro-Moratalla, A. Ribera, S. J. Blundell and P. J. Baker, *Nat. Chem.*, 2010, **2**, 1031–10

5 (a) H-B. Cui, Z. M. Wang, K. Takahashi, Y. Okano, H. Kobayashi and A. Kobayashi, *J. Am. Chem. Soc*., 2006, **128**, 15074; (b) P. Jain P., V. Ramachandran, R. J. Clark, H. D. Zhou, B. H. Toby, N. S. Dalal, H. W. Kroto and A. K. Cheetham, *J. Am. Chem. Soc.*, 2009, **131**, 13625–13627; (c) G-C. Xu, W. Zhang, X-M. Ma, Y-H. Chen, L. Zhang, H-L. Cai, Z-M. Wang, R-G. Xiong and S. Gao, *J. Am. Chem. Soc.*, 2011, **133**, 14948–14951; (d) L. Cañadillas-Delgado, O. Fabelo, J. A. Rodríguez-Velamazán, M. H. Lemée-Cailleau, S. A. Mason, E. Pardo, F. Lloret, J. P. Zhao, X. H. Bu, V. Simonet, C. V. Colin and J. Rodríguez-Carvajal, *J. Am. Chem. Soc*., 2012, **134**, 19772-19781.

6 Spin-Crossover in Transition Metal Compounds, Vols. I-III, in Topics in Current Chemistry (Eds. P. Gütlich and H.A. Goodwin), Springer, Berlin, 2004.

7 (a) A. B. Gaspar, V. Ksenofontov, M. Seredyuk and P. Gütlich, *Coord. Chem. Rev.*, 2005, **249**, 2661–2676; (b) A. Bousseksou, G. Molnár, L. Salmon and W. Nicolazzi, *Chem. Soc. Rev*., 2011, **40**, 3313–3335; (c) O. Roubeau, *Chem. Eur. J*., 2012, **18**, 15230-15244

8 P. Gütlich, A. Hauser and H. Spiering, *Angew. Chem. Int. Ed.*, 1994, **33**, 2024–2054.

9 M. C. Muñoz and J. A. Real, *Coord. Chem. Rev.*, 2011, **255**, 2068–2093.

10 (a) O. Kahn and C. J. Martinez, *Science*, 1998, **279**, 44; (b) J. A. Rodríguez-Velamazán, M. A. González, J. A. Real, M. Castro, M. C. Muñoz, A. B. Gaspar, R. Ohtani, M. Ohba, K. Yoneda, Y. Hijikata, N. Yanai, M. Mizuno, H. Ando, and S. Kitagawa, *J. Am. Chem. Soc.*, 2012, **134**, 5083−5089.

11 (a) A. Bousseksou, K. Boukheddaden, M. Goiran, C. Consejo and J. P. Tuchagues, *Phys. Rev. B*, 2002, **65**, 172-412; (b) S. Kimura, Y. Narumi, K. Kindo, M. Nakano and G. Matsubayashi, *Phys. Rev. B*, 2005, **72**, 064448

12 (a) S. Cobo, D. Ostrovskii, S. Bonhommeau, L. Vendier, G. Molnár, L. Salmon, K. Tanaka and A. Bousseksou, *J. Am. Chem. Soc.*, 2008, **130**, 9019 – 9024; (b) S. Bonhommeau, G. Molnár, A. Galet, A. Zwick, J. A. Real, J. J. McGarvey and A. Bousseksou, *Angew. Chem. Int. Ed*., 2005, **44**, 2.

13 (a) M. Ohba, K. Yoneda, G. Agustí, M. C. Muñoz, A. B. Gaspar, J. A. Real, M. Yamasaki, H. Ando, Y. Nakao, S. Sakaki and S. Kitagawa, *Angew. Chem. Int. Ed.*, 2009, **48**, 4767-4771; (b) G. Agustí, R. Ohtani, K. Yoneda, A. B. Gaspar, M. Ohba, J. F. Sánchez-Royo, M. C. Muñoz, S. Kitagawa and J. A. Real, *Angew. Chem. Int. Ed.*, 2009, **48**, 8944-8947; (b) R. Ohtani, K. Yoneda, S. Furukawa, N. Horike, S. Kitagawa, A. B. Gaspar, M. C. Muñoz, J. A. Real and M. Ohba, *J. Am. Chem. Soc*., 2011, **133**, 8600-8605.

14 (a) A. Galet, A. B. Gaspar, M. C. Muñoz, G. V. Bukin, G. Levchenko and J. A. Real, *Adv. Mater*., 2005, **17**, 2949; F. J. Muñoz-Lara, Z. Arcís-Castillo, M. C. Muñoz, J. A. Rodríguez-Velamazán, A. B. Gaspar and J. A. Real, *Inorg. Chem.*, 2012, **51**, 11126−11132; c) G. A. Craig, J. S. Costa, O. Roubeau, S. J. Teat, H. J. Shepherd, M. Lopes, G. Molnàr, A. Bousseksou, G. Aromí, *Dalton Trans*., 2014, **43**, 729-737.

15 a) X. Feng, C. Mathonière, I-R. Jeon, M. Rouzières, A. Ozarowski, M. L. Aubrey, M. I. Gonzalez, R. Clérac, J. R. Long, *J. Am. Chem. Soc.*, 2013, **135**, 15880-15884; b) R. Ababei, C. Pichon, O. Roubeau, Y-G. Li, N. Bréfuel, L. Buisson, P. Guionneau, C. Mathonière, R. Clérac, *J. Am. Chem. Soc.*, 2013, **135**, 14840-1483.

16 J. S. Miller and A. J. Epstein, *Angew. Chem. Int. Ed. Engl.*, 1994, **33**, 385–415.

17 (a) M. Clemente-León, E. Coronado, M. López-Jordà, C. Desplanches, S. Asthana, H. Wang and J-F. Létard, *Chem. Sci*., 2011, **2**, 1121–1127; (b) M. Clemente-León, E. Coronado, M. López-Jordà and J. C. Waerenborgh, *Inorg. Chem*., 2011, **50**, 9122–9130.

18 S. Ohkoshi, K. Imoto, Y. Tsunobuchi, S. Takano and H. Tokoro, *Nat. Chem.*, 2011, **3**, 564–569.

19 O. Roubeau, M. Evangelisti and E. Natividad, *Chem. Commun.*, 2012, **48**, 7604–7606. Note that a slightly lower value of T_N, at 2.2 K, is derived from calorimetric data.

20 E. F. Bertaut, In Magnetism; G. T. Rado and H. Shul Eds.; Academic: NewYork, 1963; Vol. III, Chapter 4.

21 (a) S. Kirpatrick, C. Gelatt and M. Vecci, M. *Science*, 1983, **220**, 671; (b) J. Rodríguez-Carvajal, *Mater. Sci. Forum* 2001, **378–381**, 268.

22 S. Blundell, Magnetism in Condensed Matter, Oxford Master Series in Condensed Matter (Oxford University Press, Oxford, 2001.

23 I. de Pedro, A. García-Saiz, J. Gonzalez, I. Ruiz de Larramendi, T. Rojo, C. A. M. Afonso, S. P. Simeonov, J. C. Waerenborgh, J. A. Blanco, B. Ramajo, J. Rodríguez Fernández, *Phys. Chem. Chem. Phys.*, 2013, **15**, 12724-12733

24 M. Takenaka, T. Kawakami, A. Ito, K. Kinoshita, Y. Kitagawa, S. Yamanaka, K. Yamagushi and M. Okamura, *Polyhedron*, 2011, **30**, 3284–3291.

25 In a mean-field approach and using the $-JS_iS_j$ formalism, the Weiss constant is defined as $\theta = zJS(S+1)/3k_B$, where z is the number of nearest neighbours for each spin S. For $z = 2$, as proper for the 1D stacks of $FeBr_4^-$ ions, the fit provides $\theta = 1.90$ K, thus yielding $J/k_B = 0.33$ K for the dominant intrachain exchange.

26 T. Oguchi, *Phys. Rev.*, 1964, **133**, A1098-A1099.

27 P. Panissod and M. Drillon, "*Magnetic ordering due to dipolar interaction in low dimensional materials*" in Magnetism: Molecules to Materials IV, J. S. Miller and M. Drillon Eds., Wiley-VCH 2006, pp 233-266.

28 A Metropolis Monte-Carlo calculation of the dipolar energy was performed on 3x3x7 cells with periodic boundary conditions using the positions of the Fe2 site in the structure of **1** at 10 K. Letting the spins to rotate freely within the *ab* plane and fixing S_z to 0, an energy minimum of ca. –0.50 K was reached, with the spins either in the x or y direction.

29 A. Rudavskyi, R. W. A. Havenith, R. Broer, C. de Graaf, C. Sousa, *Dalton Trans.*, 2013, **42**, 14702-14709

30 D. Bloch, *J. Phys. Chem. Solids*, 1966, **27**, 881.